AIAA JOURNAL
Vol. 44, No. 6, June 2006

Numerical Simulations of a Feedback-Controlled Circular Cylinder Wake

Stefan Siegel,* Kelly Cohen,† and Thomas McLaughlin‡
U.S. Air Force Academy, Colorado Springs, Colorado 80840

The effect of feedback flow control on the wake of a circular cylinder at a Reynolds number of 100 is investigated in direct numerical simulation. The control approach uses a low-dimensional model based on proper orthogonal decomposition (POD). The controller applies linear proportional and differential feedback to the estimate of the first POD mode. The range of validity of the POD model is explored in detail. Actuation is implemented as displacement of the cylinder normal to the flow. It is demonstrated that the threshold peak amplitude below which the control actuation ceases to be effective is in the order of 5% of the cylinder diameter. The closed-loop feedback simulations explore the effect of both fixed-phase and variable-phase feedback on the wake. Whereas fixed-phase feedback is effective in reducing drag and unsteady lift, it fails to stabilize this state once the low drag state has been reached. Variable-phase feedback, however, achieves the same drag and unsteady lift reductions while being able to stabilize the flow in the low drag state. In the low drag state, the near wake is entirely steady, whereas the far wake exhibits vortex shedding at a reduced intensity. A drag reduction of 15% of the drag was achieved, and the unsteady lift force was lowered by 90%.

Introduction

TWO-DIMENSIONAL bluff-body wakes have been investigated for quite some time. In a two-dimensional cylinder wake, self-excited oscillations in the form of periodic shedding of vortices are observed above a critical Reynolds number of approximately 47. This behavior is referred to as the von Kármán vortex street. According to Williamson,[1] the regime of laminar vortex shedding extends to a Reynolds number of approximately 180, before three-dimensional instabilities, as investigated by Karniadakis and Triantafyllou,[2] occur. This is the Reynolds number regime that we target in this investigation. However, the von Kármán vortex street as the fundamental feature of this type of wake flow is sustained to very large Reynolds numbers (on the order of millions). Therefore, a control method developed at low Reynolds numbers will still be applicable to the von Kármán vortex street aspect of flows at much higher Reynolds numbers, where additional problems such as turbulence and three dimensionality will have to be dealt with. Conversely, without being able to control successfully the Kàrmàn vortex street at low Reynolds numbers, it would be very difficult to control this flow at high Reynolds numbers.

The nonlinear oscillations of the vortex street lead to some undesirable effects associated with unsteady pressures such as fluid–structure interactions[3] and lift/drag fluctuations.[4] Also, the vortices themselves greatly increase the drag of the bluff body, compared to the steady wake that can be observed at lower Reynolds numbers. Monkewitz[5] showed that the von Kármán vortex street is the result of an absolute, global instability in the near wake of the cylinder. Farther downstream, the flow is convectively unstable. This absolute instability is causing the flow to behave as a self-sustained oscillator, with internal positive feedback leading to temporal amplification of the oscillation by the recirculation region downstream of the cylinder.

Many attempts have been made to improve the unsteady vortex street. When active open-loop forcing of the wake is employed, the vortex shedding in the wake can be locked in phase to the forcing signal.[6] Whereas these findings suggest that the dominant structures in the flowfield can be influenced by the forcing, it also strengthens the vortices and, consequently, increases the mean drag as well as unsteady lift forces. Different forcing methods are effective in influencing the behavior of the flow. Acoustic excitation of the wake; longitudinal, lateral, or rotational vibration of the cylinder model; and alternate blowing and suction at the separation points[5] have been used. When these excitation methods are used, the flow exhibits regions of lock-in and non-lock-in. Koopmann[7] experimentally investigated these regions and found that the lock-in frequency range depends on the forcing amplitude. The higher the forcing amplitude, the larger the frequency band was for which he could achieve lock-in. Additionally, even at the natural vortex shedding frequency, he found a minimum threshold amplitude that was needed for lock-in to occur.

None of these open-loop forcing methods have been shown to reduce the drag, independent of frequency and amplitude employed. The only exceptions are situations where the separation point location is shifted. Note that the geometry of a circular cylinder lends itself to active control methods that target the separation point location of the flow rather than the absolute instability of the wake itself. When methods such as periodic blowing and suction on the cylinder surface are used in a fashion similar to that employed on the suction side of airfoils, the separation point can be moved aft, which in turn will lead to a narrower wake. A narrower wake will exhibit improved stability characteristics in addition to lower drag due to a lower velocity deficit in and by itself. This effect can be observed in the natural cylinder wake during the drag crisis, when laminar–turbulent boundary-layer transition occurs upstream of the separation point and the resulting turbulent boundary layer keeps the flow attached longer, shifting the separation point downstream. Thus, feedback control investigations using periodic blowing and suction such as that employed by Min and Choi[8] actually employ two flow control techniques simultaneously, namely, separation control and wake stabilization due to feedback. It is difficult if not impossible to judge what portion of the improvement is due to either of these techniques in their simulations.

The only way of suppressing the self-excited flow oscillations without altering the mean flow is by the incorporation of active closed-loop flow control.[9] Traditionally, several fundamentally different approaches to achieve feedback flow control have

Presented as Paper 2003-3569 at the AIAA Fluid Dynamics Conference, Orlando, FL, 23–26 July 2003; received 7 August 2003; revision received 11 April 2005; accepted for publication 4 November 2005.

*Assistant Research Associate, Department of Aeronautics. Senior Member AIAA.
†Contracted Research Engineer, Department of Aeronautics. Senior Member AIAA.
‡Director, Aeronautics Research Center, Department of Aeronautics. Associate Fellow AIAA.

been employed. The mathematically driven approach to develop a control scheme is hampered by the complexity of the governing Navier–Stokes equations. To tackle this complexity, one needs to make simplifying assumptions. At this point, the assumptions made in simplifying the equations have often rendered the results inapplicable to real life experiments.[10] If no simplifications or assumptions are made, however, the resulting control algorithm (if it can be derived at all with today's computing capabilities) is often too complex to be implemented in real time.[11]

However, approaching the controls problem using an experimental/empirical approach without any modeling of the physics of the flow also yields unsatisfactory results. Experimental studies conducted by Roussopulos show that a linear proportional feedback control based on a single sensor feedback is able to delay the onset of the wake instability only slightly, rendering the wake stable at Reynolds number about 20% higher than the unforced case. Roussopulos[3] reports that, above $Re = 60$, a single-sensor feedback may suppress the original mode but destabilizes one of the other modes. Therefore, better control strategies are needed to stabilize the wake at Reynolds numbers of technical interest.

The solution to this problem lies in the development of a low-order model of the flow. The model can be used both for controller development, as well as flowfield state estimation. Ideally, it reduces the complexity of the governing Navier–Stokes equations to a level that the model can be implemented in real time, while still capturing the important physics of the flow. Pioneering work in the development of low-dimensional models was performed by Deane et al.[12] Gillies[13] applied this technique to cylinder wakes by developing a low-dimensional model of the cylinder wake at a Reynolds number of 100. Cohen et al.[14] have shown that, using this model, the cylinder wake model flow can be successfully controlled using a relatively simple linear control approach based on the most dominant mode only. Ma and Karniadakis[15] extended the model development to address the three-dimensional features present in cylinder wakes at Reynolds numbers higher than 180.

Whereas this research addresses a rigidly mounted cylinder that is translated according to the feedback control law, the reduction in unsteady lift forces that are sought ultimately addresses problems encountered in fluid–structure interaction research. In fluid–structure interaction problems such as the cable simulations investigated by Newman and Karniadakis,[16] an unsteady lift force induces an oscillation of a flexible cable. Feedback flow control may be used to reduce the unsteady lift force, thus, limiting the response of the flexible structure.

The goal of this effort is to apply the approach developed by Cohen et al.[14] to a full Navier–Stokes simulation of the flowfield. A limited number of sensors placed in the wake are used to estimate the state of the flow that is characterized using a low-dimensional model. The controller then acts on the flow state estimates to determine the actuator displacement. (Figure 1 shows the overall setup of this experiment.)

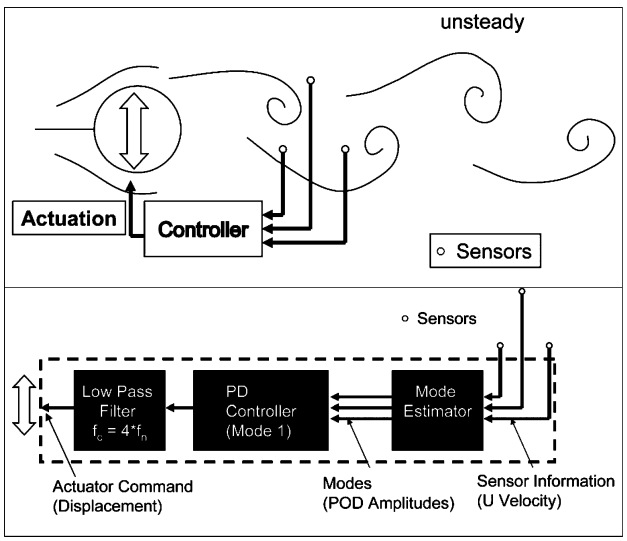

Fig. 1 Feedback control setup.

Numerical Methods

We employ numerical methods in this paper both to simulate the flowfield, which is detailed in the following section, as well as to accomplish feedback. The latter methods are detailed in the sections on proper orthogonal decomposition (POD) as well as on the controller.

Computational Fluid Dynamics Model

For the numerical simulations, Cobalt Solutions's Cobalt solver version 2.02 was used. Cobalt is a commercial finite volume method developed for solution of the compressible Navier–Stokes equations and is described by Strang et al.[17] The numerical method is a cell-centered finite volume approach applicable to arbitrary cell topologies, for example, hexahedra, prisms, tetrahedral. The spatial operator used the exact Riemann solver of Gottlieb and Groth,[18] least-squares gradient calculations using quadratic regulator factorization to provide second-order accuracy in space, and total variation diminishing flux limiters to limit extremes at cell faces. A point-implicit method using analytic first-order inviscid and viscous Jacobians is used for advancement of the discretized system. For time-accurate computations, a Newton subiteration scheme is employed, and the method is second-order accurate in time. For parallel performance, Cobalt uses the domain decomposition library ParMetis[19] to provide nearly perfect load balancing with a minimal surface interaction between zones. Communication between processors is achieved using message passing interface, with parallel efficiencies above 95% on as many as 1024 processors.[20] Boundary conditions at the far field are implemented as Riemann invariants, with the static pressure fixed, and the remaining flow primitives are free to float. The cylinder surface is modeled as an adiabatic nonslip boundary. Simulation of rigid-body motion is achieved through an arbitrary Lagrangian Eulerian (ALE) formulation, where the gird is neither stationary nor follows the fluid motion. The conservation equations are solved in an inertial reference frame, but the spatial operator is modified so that the advection terms are relative to the (noninertial) grid-reference frame. This requires simple modifications to many boundary conditions and to the initial conditions for the Riemann problem. The inviscid and viscous work terms due to the grid velocity must also be removed from the spatial operator. The ALE formulation also forces certain modifications to the time-centered implicit temporal operator. At the beginning of a time step, all geometric quantities are transformed to their values at the end of the given time step, according to the specified motion. This ensures the fluxes, which an implicit scheme computes at the end of the time step, are consistent with the geometry. Such quantities include centroid locations and least-squares weights vectors, but because the motion is rigid, volume and area are invariant under the transformation. A number of Newton subiterations are used to reduce errors associated with integrating over the time step with an implicit temporal operator. The method has been applied to a pitching prolate spheroid[21] and a spinning forebody[22] with good agreement to experiments.

For all investigations, an unstructured two-dimensional grid with 63,700 nodes/31,752 elements was used (Fig. 2). The grid extended from -16.9 cylinder diameters to 21.1 cylinder diameters in the x (streamwise) direction and ± 19.4 cylinder diameters in the y (flow normal) direction. The boundary conditions at the far field were Riemann invariant; at the cylinder surface an adiabatic no-slip wall boundary condition was implemented.

Cobalt allows for the specification of advection and diffusion damping coefficients, which are nondimensional with a range from zero to one. Their purpose is to resolve potential instability problems in the solver at the cost of numerical accuracy. In the limiting case of zero, no artificial damping is added. For the present investigation, an advection coefficient of 0.01 and a diffusion coefficient of 0.0 were used. Other pertinent simulation parameters are Reynolds number $Re = 100$, 32 iterations for matrix solution scheme, 3 Newton subiterations, and nondimensional time step $\Delta t^* = \Delta t \cdot U/D = 0.05$.

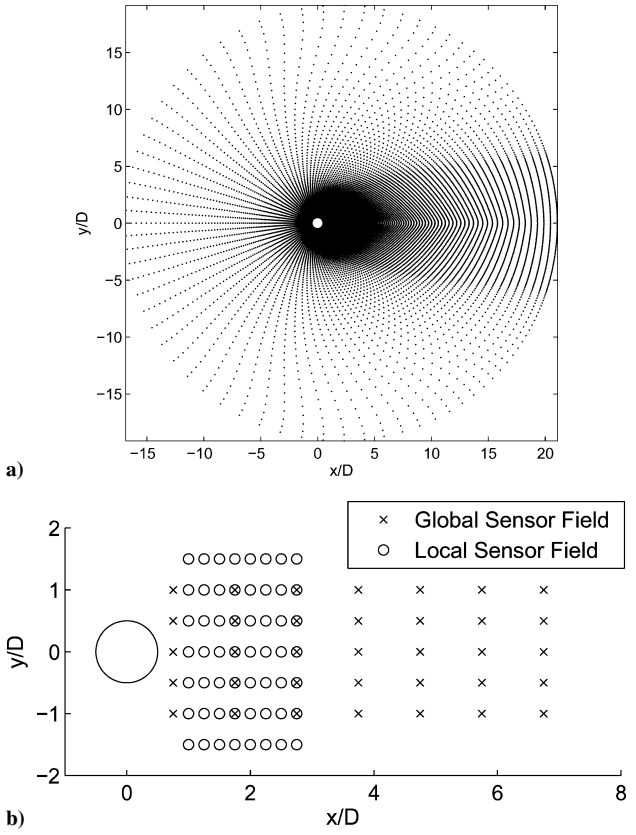

Fig. 2 Flow simulation: a) computational grid and b) sensor locations.

The simulation was triggered by skewing the incoming mean flow by $\alpha = 0.5$ deg at the first time step to introduce an initial perturbation. This breaks the symmetry of the flow and accelerates the development of the limit cycle. A grid- and time-resolution study showed good convergence for the simulation parameters outlined. For further validation of the unforced cylinder wake computational fluid dynamics (CFD) model at $Re = 100$, the resulting value of the mean drag coefficient c_d was compared to experimental and computational investigations reported in the literature. At $Re = 100$, experimental data, reported by Oertel[23] and Panton,[24] point to c_d values ranging from 1.26 to 1.4. Furthermore, Min and Choi[8] report on several numerical studies that obtained drag coefficients of 1.35 and 1.337. The Cobalt CFD model used in this effort results in a $c_d = 1.35$ at $Re = 100$, which compares well with the reported literature. Another important benchmark parameter is the nondimensional vortex-shedding frequency, the Strouhal number (Sr) for the unforced cylinder wake. Experimental results at $Re = 100$, presented by Williamson,[1] show Strouhal numbers ranging from 0.163 to 0.166. The Strouhal number obtained from the Cobalt CFD model used in this effort is $Sr = 0.163$ at $Re = 100$, which also compares well.

The simulations were performed on a Beowulf Linux cluster consisting of 64 Pentium 3 processors operating at 1 GHz. When run on 8 processors, typically a time step took on the order of 6 s to compute. Employing larger number of processors yielded disproportionately small improvements in execution time, due to network and disk access overhead for saving the results at the end of each time step.

POD Modeling and Estimation

Feasible real-time estimation and control of the cylinder wake may be effectively realized by reducing the model complexity of the cylinder wake, as described by the Navier–Stokes equations, using POD techniques. POD, a nonlinear model reduction approach, is also referred to in the literature as the Karhunen–Loeve expansion (see Ref. 25). The desired POD model contains an adequate number of modes to enable modeling of the temporal and spatial characteristics of the large-scale coherent structures inherent in the flow.

In this effort, the method of snapshots introduced by Sirovich[26] is employed to generate the basis functions of the POD spatial modes from the numerical solution of the Navier–Stokes equations obtained using Cobalt. In all, 200 snapshots were used, equally spaced 4% of a shedding cycle apart. Thus, eight full shedding cycles contributed to the mode construction. The time interval between snapshots is five times the simulation time step. The snapshots were taken after ensuring that the cylinder wake reached steady state. Only the U velocity component (in the direction of the mean flow) was used for POD decomposition in this effort. This decision was made to be able to estimate the mode amplitudes based on sensor information, which in future experiments will yield the U and V component of velocity. Because the change in mean flow distribution is an important quantity, we chose the U velocity component over the V velocity component. We found that more than 99.98% of the kinetic energy of the flow lies in the first eight modes, with more than 93.5% in the first four modes. An important aspect of reduced order modeling concerns truncation: How many modes are important and what are the criteria for effective truncation?

The answer to the preceding question has been addressed by Cohen et al.[14] This effort showed that control of the POD model, of the von Kármán vortex street in the wake of a circular cylinder at $Re = 100$, is enabled using just the first mode. Furthermore, feedback based on the first mode alone suppressed all of the other modes in the four-mode POD model, indicating that higher-order modes derive from the fundamental modes. In view of this result, truncation of the POD model took place after the first four modes. Note the difference between the number of modes required to reconstruct the flow vs the number of modes required to control the flow. In this effort, we are interested in estimating only those modes required for closed-loop control. On the other hand, an accurate reconstruction of the velocity field based on a low-dimensional model may be obtained using between four and eight modes.[27] The POD algorithm was applied to the fluctuating velocity component in the direction of the flow, u, as shown in Eq. (1). The decomposition of this component of the velocity field is as follows:

$$\tilde{u}(x, y, t) = U(x, y) + u(x, y, t) \tag{1}$$

where U is the mean flow velocity (meters per second) and u is the fluctuating component (meters per second) that may be expanded as

$$u(x, y, t) = \sum_{k=1}^{n} a_k(t)\phi_i^{(k)}(x, y) \tag{2}$$

where $a_k(t)$ is the time-dependent coefficients (meters per second) and $\phi^{(k)}(x, y)$ are the nondimensional spatial eigenfunctions (Fig. 3) determined from the POD procedure. The first four modes of the POD decomposition are shown, plus a fifth mode that was derived by subtracting the mean freestream velocity from the mean flow distribution of the unforced flowfield. This mode was found to be necessary to obtain an estimate of the effect of feedback flow control onto the mean flow. It is being used to both estimate the effectiveness of the controller, as well as to allow for gain scheduling to account for changes in the flow receptivity to forcing in a real-time fashion. Noack et al.[28] have shown that adding a similar mode, which they refer to as the shift mode, accounts for changes in the mean flow. It greatly improves the ability of the model to account for transient effects in the flowfield. We will show the correlation between the mean flow mode and the wake drag in the following section.

Once the spatial POD eigenfunctions have been derived, the corresponding time-dependent coefficients $a_k(t)$, or mode amplitudes, need to be calculated. For this, two different schemes are reported in literature. Most often a Galerkin projection is used, which involves projecting the spatial eigenfunctions onto the Navier–Stokes equations. This process involves spatial derivatives of the snapshots, which are, particularly in the case of experimental data, inherently sensitive to noise. Gillies[9] used a simple least-squares fit, which we found to be much more robust. Whereas we employ the least-square fit in the CFD simulations, the experiment will make use of linear stochastic estimation (LSE) to estimate the mode amplitudes in real time. This estimation scheme, introduced by Adrian,[29] predicts the temporal mode amplitudes of the POD modes from a finite set of

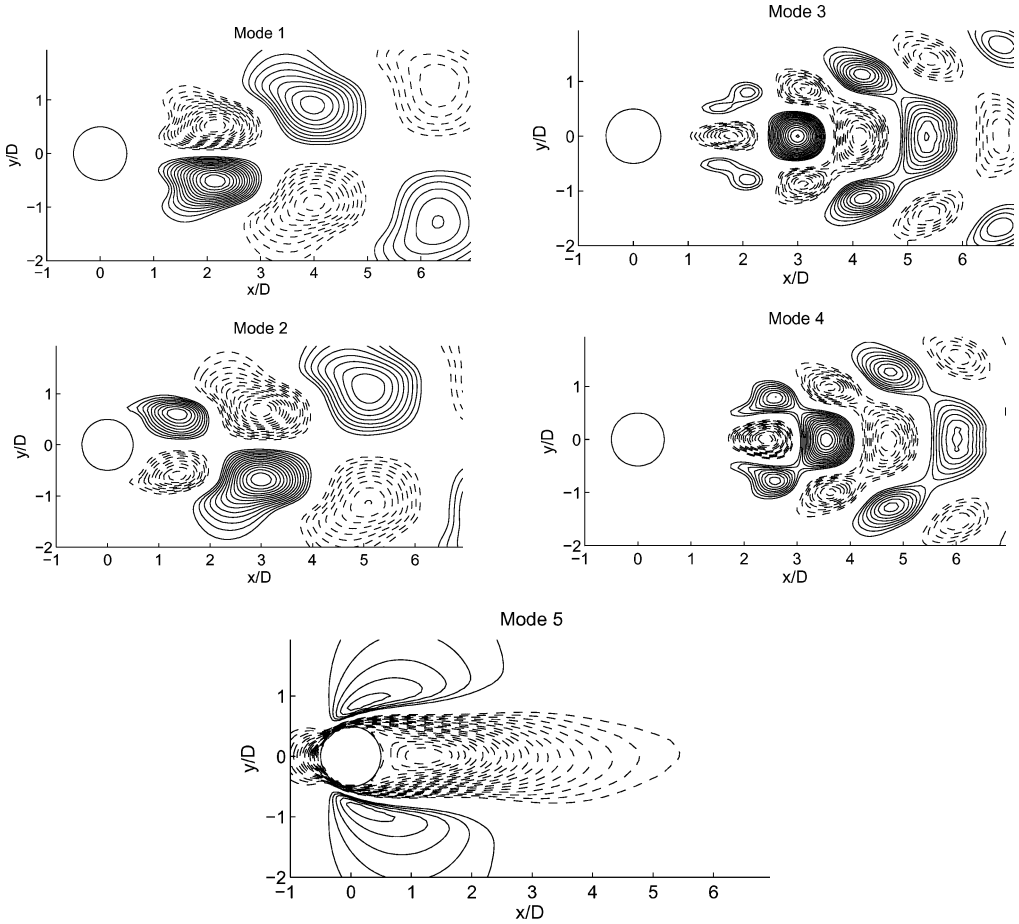

Fig. 3 Eigenfunctions of the five-mode POD model based on CFD data at $Re = 100$, using U velocity component as input for POD decomposition: flow from left to right, cylinder located at (0, 0) with diameter of 1.

measurements, which are used to develop a linear mapping from sensor readings to mode amplitudes. Because this mapping matrix is developed offline, mode estimation during a feedback control run is reduced to a simple matrix multiplication. LSE is, therefore, deterministic in terms of computing time, whereas least-square fitting is not. Thus, LSE is a much better choice for real-time implementation. Further details of stochastic estimation of POD modes are provided by Bonnet et al.[30]

For the feedback controlled runs, the CFD solver writes sensor information at requested (x, y) locations in the flow to a file after calculating a time step and then waits for an external control algorithm to update the file with the new control command for the next time step. The two different sensor grids employed for all simulations are shown in Fig. 2b and employ a total of 35 or 56 sensors in the near wake of the cylinder. The main advantage of the global sensor grid over the local grid investigated is in its ability to provide an estimate of the mode amplitudes that shows little error compared to using all grid points for mode estimation. This holds true both for the unforced case as well as the feedback-controlled cases.

Although no extensive efforts to optimize the sensor locations was undertaken, we compared the local uniformly spaced sensor field with 56 sensors between $x/D = 1$ and $x/D = 2$ to the more widely spaced, global configuration extending from $x/D = 0.75$ to $x/D = 1.75$. Whereas both grids performed well in estimating the unforced flowfield, for the feedback-controlled flow state, the local grid develops large phase and amplitude errors as soon as the flow responds to the forcing. We discuss the effect of sensor placement on estimation error in more detail in the result section for the variable-phase feedback.

Controller

Figure 1 shows the controller block diagram. The main components are a mode estimator, a proportional and differential (PD) controller, and a low-pass filter with a corner frequency of four times the natural-shedding frequency. The Cobalt CFD solver has the ability to perform rigid-body motion of a given grid. This feature was used to perform both periodically forced and feedback-controlled simulations with one degree of freedom. For all investigations, only displacement of the cylinder in the flow normal y direction was employed for forcing the flow. The control algorithm acts on the estimate of the mode 1 amplitude only. This design decision was made based on our earlier investigations controlling a low-dimensional model of the flow. For the low-dimensional model, proportional gain applied to mode 1 was sufficient to suppress vortex shedding. Because our CFD simulations require a filter to avoid feeding back small amounts of noise, we employed a PD feedback control strategy:

$$y_{\text{cyl}} = K_p \cdot a_1 + K_d \cdot \frac{\mathrm{d}a_1}{\mathrm{d}t} \tag{3}$$

Instead of directly specifying the K_p and K_d gains, these can be expressed in terms of an overall gain K and a phase advance φ:

$$K_p = K \cdot \cos(\varphi), \qquad K_d = K \cdot \sin(\varphi)/2\pi f \tag{4}$$

with f being the natural vortex-shedding frequency.

During the course of the investigations, we found it advantageous to implement a variable-gain strategy. The basic idea is that as the flowfield is modified from its original state, different values for the phase advance φ and the gain K may be more advantageous than those effective in controlling the unforced flowfield:

$$K = K_0 + K_A(a_5 - a_5|_{t=0}), \qquad \varphi = \varphi_0 + K_\varphi(a_5 - a_5|_{t=0}) \tag{5}$$

Equation (5) details the adjustment scheme for the variable-gain strategy. Because mode 5 is a good measure of the change in the

mean flow, the feedback gain K and/or phase advance φ are adjusted from their initial values K_0 and φ_0 in proportion to the change in mode 5 by applying a phase-advance factor K_φ and/or a gain-change factor K_A. These additional factors can be applied either together or individually.

Physically, the control algorithm was implemented in MATLAB® on a separate personal computer running Windows. It interfaced to the Beowulf cluster running Cobalt using Windows file sharing through Samba to read the sensor information and update the cylinder displacement.

Results

Before closed-loop feedback-flow control is employed, it is important to investigate the dynamics of the unforced flowfield in detail. Equally important, the effect of open-loop forcing needs to be understood because the receptivity of the flow to forcing will manifest itself in these investigations. The following section will outline the results of these investigations and also show the limitations of the type of forcing employed as well as the limits of the flow improvements that may be obtained using feedback control.

The following two sections will highlight a few select cases of the unforced flow, open-loop forced flow, and feedback-controlled flow. Two different kinds of feedback control were employed: one using a fixed set of PD gains and one set where the gains were varied depending on the change in the mean flow. The latter is usually referred to as a gain-scheduling scheme.

Unforced Wake Properties

In a CFD simulation, the flowfield is started abruptly at time zero. Figure 4 shows the evolution of the flowfield after this startup. The flow evolves from a Stokes-type streamline pattern at $t = 0$ s (Fig. 4a) through a steady wake with two closed recirculation bubbles at $t = 0.4$ s (Fig. 4b) into the steady state showing the unsteady von Kármán vortex street at $t = 2.94$ s (Fig. 4d). During this startup, the flow reaches a state of minimum drag at $t = 0.7$ s (Fig. 4c). This minimum drag coincides with a maximum amplitude of mode 5 (the freestream mode), as well as a maximum mean recirculation zone length with the downstream end of the recirculation zone located at $x/D = 5.4$ (not depicted). Note that the minimum drag does not coincide in time with the steady wake as one might expect, but rather with a vortex-shedding pattern with a very large wavelength, as shown in Fig. 4c. The total drag in this situation is about 16% less than in the steady-state vortex-shedding situation. Thus, one may argue that a feedback-control scheme aiming to suppress the vortex shedding may at best recover up to this portion of the total drag. We refer to this 16% portion of the overall drag force as the vortex-induced drag because it is caused by the vortex shedding in the unsteady wake flow. It is a portion of the pressure drag. About 2 s after the startup of the simulation, the wake approaches a time-periodic vortex-shedding state. The mean recirculation zone ends at $x/D = 1.9$ in this final flow state.

Open-Loop Forced Wake Properties

The cylinder wake flow can be forced in an open-loop fashion using sinusoidal displacement of the cylinder with a given amplitude and frequency. Koopmann[7] investigated the response of the flow to this type of forcing in a wind-tunnel experiment. He found a region around the natural vortex-shedding frequency where he could achieve lock-in, which is characterized by the wake responding to the forcing by establishing a fixed-phase relationship with respect to the forcing. The frequency band around the natural vortex-shedding frequency f_0 for which lock-in may be achieved is amplitude dependent, as shown in Fig. 5a. Inside the V-shaped area, the flow responds to the forcing with a fixed-phase relationship, with the vortex shedding in phase with the forcing. Outside, the response to

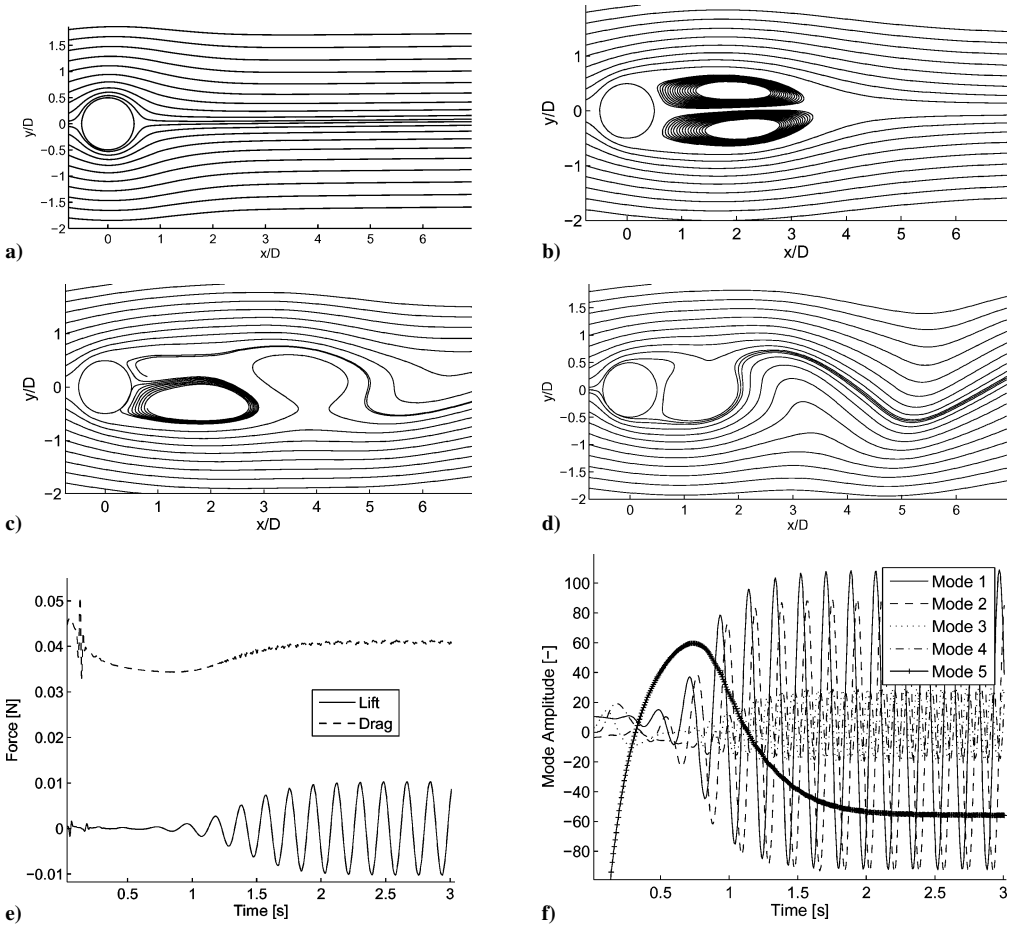

Fig. 4 Evolution of flowfield: instantaneous streamlines at a) $t = 0.0$, b) $t = 0.4$, c) $t = 0.7$, and d) $t = 3.0$ s after simulation startup, e) lift and drag during simulation startup, and f) mode amplitudes during simulation startup.

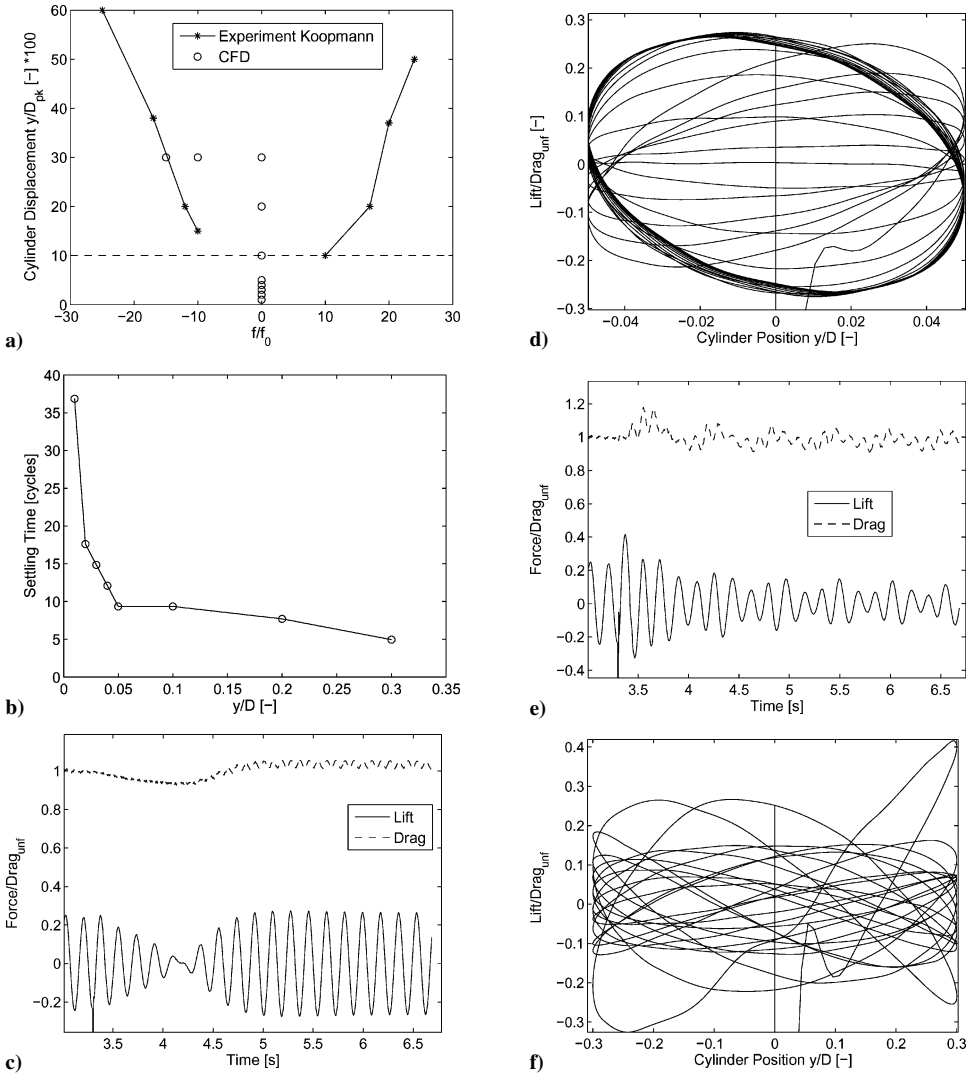

Fig. 5 Open-loop forced simulations: a) lock-in region adapted from Koopmann,[7] b) settling time for different forcing amplitudes using sinusoidal forcing at natural-shedding frequency, diameter, c) lift and drag and d) phase plot nondimensional lift force vs cylinder motion, with sinusoidal forcing at natural frequency using amplitude of 5% of cylinder diameter, and e) lift and drag and f) phase plot lift vs cylinder motion, with sinusoidal forcing at 75% of natural frequency using amplitude of 30% of cylinder diameter.

forcing is chaotic. In general, the larger the amplitude, the larger the frequency band is for which lock-in is possible. However, a threshold amplitude exists below which the flow will not respond to the forcing any more. In Koopmann's experiment, this amplitude was at $y/D = 10\%$.

We resampled the lock-in region in the CFD simulation at select amplitude and frequency pairs shown in Fig. 5a. The simulations always activated the forcing at the same time, 3.3 s after the start of the simulation, which resulted in the forcing being 180 deg out of phase with the vortex shedding. A typical run resulting in lock-in is shown in Figs. 5c and 5d. Figure 5c shows that the flowfield goes through a transient phase before lock-in is achieved after about nine shedding cycles. After the transient, a fixed-phase relationship between forcing and the unsteady lift force induced by the vortex shedding is established, as shown in Fig. 5d. We refer to the time during which the flow adjusts to the forcing as the settling time. For comparison, Figs. 5e and 5f show the chaotic response of the flow to a forcing input characterized by a frequency/amplitude combination just outside the lock-in range. The flow does not establish a fixed-phase relationship to the forcing in that case. A scan through different forcing amplitudes was performed at the natural-shedding frequency, $f/f_0 = 1$, with amplitudes ranging from 1 to 30% of the cylinder diameter. The settling times observed in these cases are shown in Fig. 5b. Whereas the settling times are roughly constant for forcing amplitudes between 5 and 10%, for smaller amplitudes a drastic increase in settling times can be observed. This manifests the behavior observed by Koopmann around 10% forcing amplitude, albeit shifted toward somewhat smaller amplitudes. There are two possible explanations for this. Koopmann used spanwise coherence as an indicator for lock-in, which may occur at larger amplitudes than the local lock-in observed in our two-dimensional simulations. Additionally, his experiment was conducted in a wind-tunnel environment, which features more mean flow turbulence than the CFD simulations. This would also tend to increase the amount of forcing needed to overcome the turbulence and achieve lock-in.

The open-loop forcing results have important implications for the closed-loop feedback control runs. Because our POD model is based on unforced flowfield data, it can capture only flow behavior that is phenomenologically similar to the unforced wake. In terms of the lock-in region, this flow behavior is encountered as long as the controller keeps the flow within the lock-in region. The chaotic behavior at off-natural frequencies is clearly not modeled in the POD modes. More important, if the displacement of the cylinder becomes smaller than about 5% of the cylinder diameter, the flow will no longer be responsive to the forcing.

Fixed-Phase Feedback

A series of simulations with different phase advance φ were conducted. The overall gain K was kept constant at a value that resulted in initial displacements of less than 15% of the cylinder diameter, to avoid strongly nonlinear effects that have been reported in the

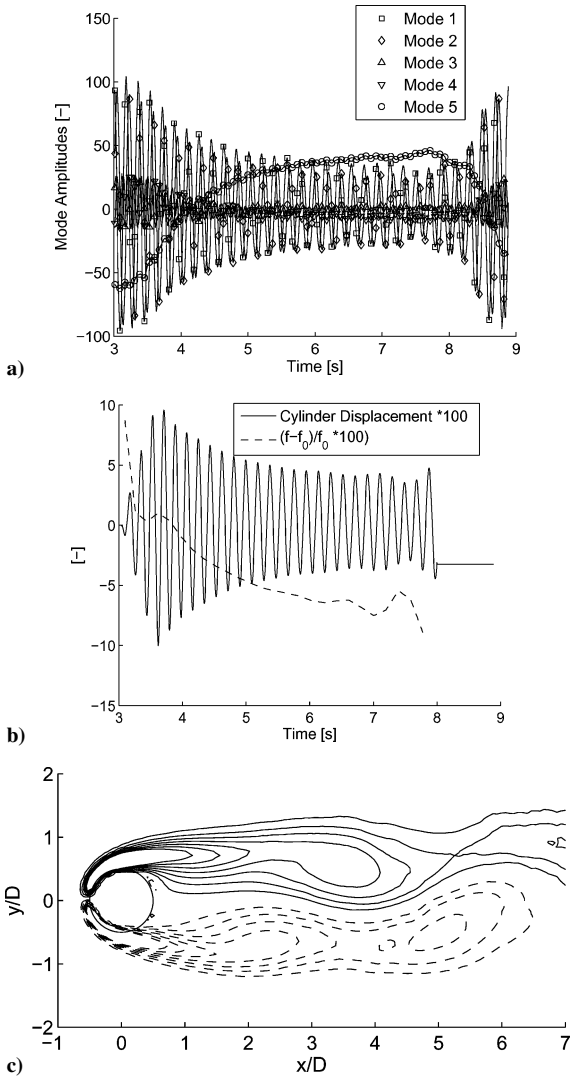

Fig. 6 Linear fixed-gain feedback with gain $K = 1e-3$, phase $\varphi = 45$ deg, controller activated at 3.03 s and deactivated at 8 s: a) mode amplitudes, b) cylinder displacement and frequency, and c) instantaneous vorticity contours at $t = 6.5$ s.

literature at higher amplitudes.[31] Qualitatively, the runs resulted in either an increase or a decrease of the mode amplitudes. A case with a decrease in mode amplitudes is shown in Fig. 6. During the control run, the global mode amplitude of mode 1 decreases from a peak value of around 100 to a peak value of less than 40. This decrease in mode amplitude does not apply just to mode 1, but also to mode 2 and the two higher-order modes. These findings are consistent with our experience in controlling a low-order model of the flow,[14] where a similar coupling between the modes could be observed. When the behavior of the unsteady lift and the drag is considered, a reduction in drag of about 14% of the unforced drag was observed, whereas the unsteady lift was reduced by about 50%. Comparing the drag reduction of 14% to the minimum drag encountered during startup of the CFD simulation, which is 16% less than the drag of the unforced flowfield, we find that the simple feedback controller with a fixed gain and phase recovers more than 87% of the vortex-induced drag. However, all of the fixed-phase simulations that led to a drag reduction were not able to stabilize the flow at a low drag value. In Fig. 6a, at a time of 7.5 s, a reduction followed by an increase in mode amplitude can be observed. This is the first indication of the onset of an instability that will ultimately render the flowfield chaotic, if the simulation is continued.

When the cylinder displacement is inspected during this simulation (Fig. 6b), the onset of the instability coincides with a cylinder displacement that has just dropped below 5% of the cylinder diameter. Thus, the onset of the instability coincides with the loss of flow response found in the periodically open-loop forced runs discussed in the preceding section. The instantaneous vorticity contours shown in Fig. 6c show a wake flow where the vortices form farther downstream of the cylinder, compared to the streamlines of the unforced flow shown in Fig. 4d. In the unforced flow, the vortices roll up between 1 and 2 diameters downstream of the cylinder, whereas in the feedback-controlled situation, the rollup occurs between 3 and 4 diameters downstream. As a result, the reverse flow region is lengthened, from $x/D = 1.9$ in the unforced case to $x/D = 4.3$. Simultaneously with the lengthening of the recirculation zone, we observe a reduction in the vortex-shedding frequency. The correlation between the shedding frequency and the reduction in drag is in qualitative agreement with the wake model proposed by Ahlborn et al.[32]

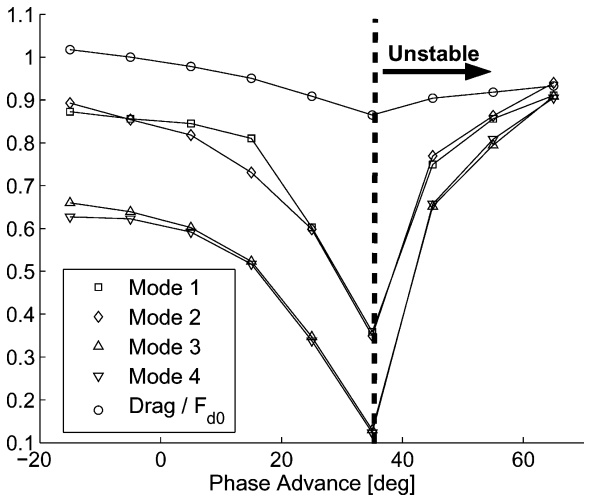

Fig. 7 Mode amplitudes and drag force for various fixed-phase advance angles; feedback with fixed gain $K = 1e-6$.

A summary of the effect of different amounts of fixed-phase advance between mode 1 and the cylinder motion on both the mode amplitudes and the drag force is shown in Fig. 7. Whereas it is apparent that the largest drag and mode amplitude reductions are achieved for a phase advance of about 35 deg, this phase advance is also unstable over longer time periods. The good correlation between the mode amplitude reduction and the drag reduction suggests a strong link between these quantities. Also, it can be seen that all mode amplitudes experience a reduction, which shows the coupling between the modes to be strong. Also note that a 0-deg phase advance has no impact on the drag.

With these findings on the impact of fixed-phase feedback on the wake, an important question to be asked is, if the wake can be stabilized at a low-mode amplitude, and if so, how? An obvious parameter to adjust to achieve this is the gain of the controller. This led to the implementation of a variable-gain controller as outlined in the description of the control algorithm, whose impacts on the wake are described in the following section.

Variable-Phase Feedback

When the overall feedback gain K is increased using a suitable adjustment factor K_A in accordance with Eq. (5), larger cylinder displacements, which would ensure the ability to control the wake at small-mode amplitude, can be achieved. However, we found that larger gains do not stabilize the wake, but rather lead to a low-frequency oscillation and instability even when the cylinder displacements are kept above 5% of the cylinder diameter. This is demonstrated in Fig. 8, where the phase of the feedback is kept constant at 50 deg while the overall gain K is increased as the fluctuating mode amplitudes decrease: The parameters for Eq. (5) are $K_0 = 1e-3$, $\varphi_0 = 50$ deg, $K_A = 2e-6$, and $K_\varphi = 0$ deg. This allows for the actuation amplitude to be maintained above 5%, which is a necessary requirement for controllability as outlined in the open-loop results section. Nonetheless, the flow becomes unstable despite

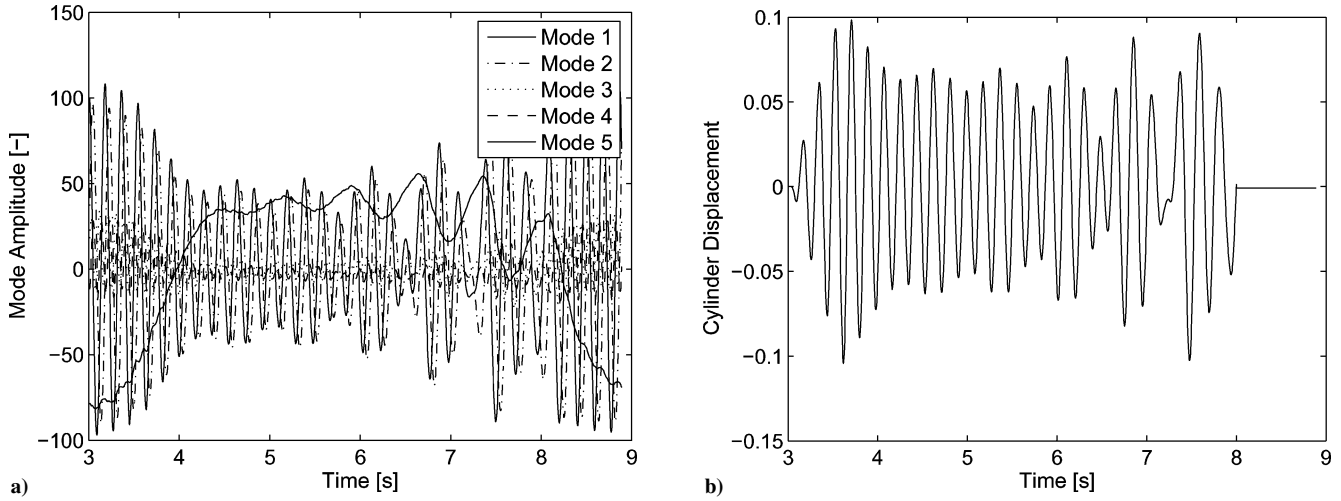

Fig. 8 Mode 1 linear feedback with variable-gain parameters $K_0 = 1e-3$, $\varphi_0 = 50$ deg, $K_A = 2e-6$, and $K_\varphi = 0$ deg: a) mode amplitudes and b) cylinder displacement.

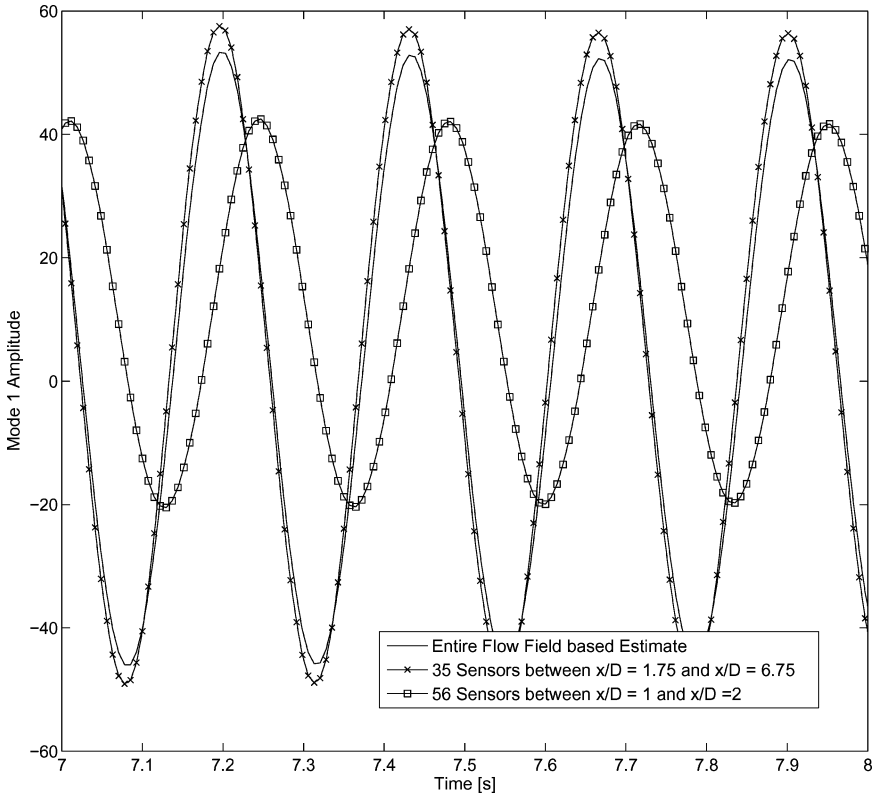

Fig. 9 Actual mode 1 amplitudes compared to sensor-based estimates using different sensor placement methods. Variable-gain feedback-controlled flow estimated flowfield.

this elevated minimum amplitude while the controller is active, which is between 3.03 and 8 s. A low-frequency oscillation can be observed in the fluctuating modes, but is most clearly evident in the mean flow mode 5. This oscillation ultimately destabilizes the control scheme. To achieve wake stabilization at a low drag level, one other parameter can be considered for adjustment, the phase of the feedback.

During an investigation into different sensor configurations, we used the local sensor field shown in Fig. 2b. As was later discovered, this sensor field developed a large estimation error with respect to the phase error of the mode 1 estimate, relative to an estimate based on the entire flowfield, as shown in Fig. 9, where both sensor fields are evenly distributed in x and y with an extent of ± 1 diameters in the y direction, but cover a small or large range in the x direction. In addition, a variable-feedback gain and phase were used according to Eq. (5), with feedback parameters of $K_0 = 1e-3$, $\varphi_0 = 15$ deg, $K_A = 1e-6$, and $K_\varphi = 0.75$ deg. The controller was activated at 3.03 s and deactivated at 8 s, after which the wake resumed the original unforced vortex shedding. With the controller active, the wake stabilized at an overall drag reduction of about 15% with an unsteady lift amplitude reduction of 90% (Fig. 10c), compared to the unforced flowfield. Inspecting the resulting feedback phase caused by both the estimation error and the variable-gain feedback shown in Fig. 10f, one can see that the phase advance is reduced to almost zero in the stabilized state case. This phase advance angle stabilizes the flowfield at a low level of vortex shedding, with the recirculation length extended to $x/D = 3.95$, or more than twice the unforced length. Figure 10d demonstrates that the wake develops a new limit cycle at a reduced mode 1 amplitude in the feedback-controlled stabilized case. Note that, when applied from the moment

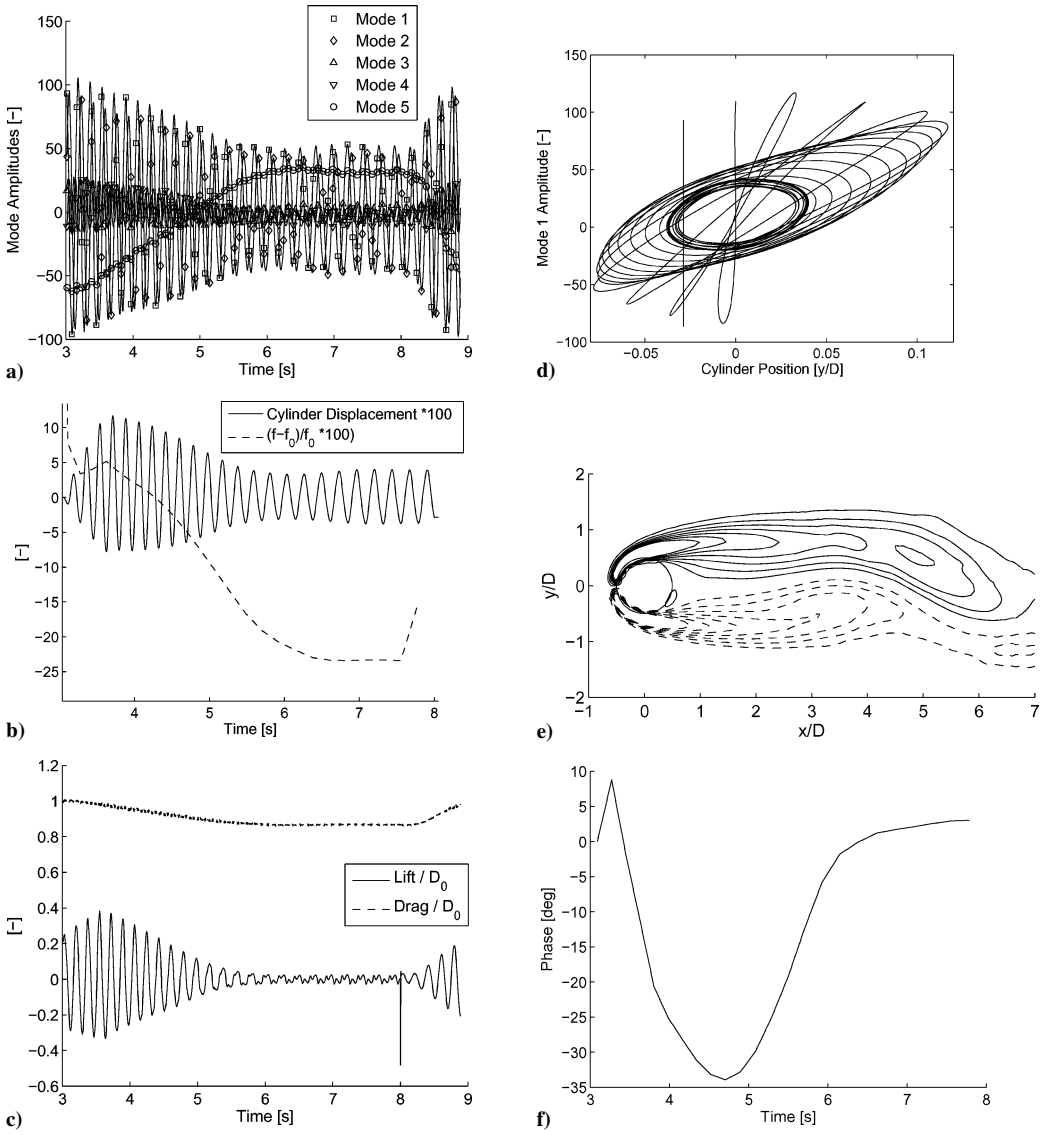

Fig. 10 Linear feedback of mode 1 with variable gain controller, $K_0 = 1e-3$, $\varphi_0 = 15$ deg, $K_A = 1e-6$, and $K_\varphi = 0.75$ deg: a) mode amplitudes, b) cylinder displacement and frequency, c) lift and drag, d) phase between cylinder position and mode 1, e) instantaneous vorticity contours at $t = 7.5$ s, and f) phase advance during the run.

the controller is activated, a 0-deg phase shift does not lead to a reduction in vortex-shedding strength, but rather phase locks the wake at a vortex-shedding level that is comparable to the unforced flowfield, as shown in the fixed-phase feedback result section. Thus, a positive feedback phase is needed to reduce the shedding strength, but after reduction, a zero feedback phase is effective in stabilizing the shedding at this level. Other phase angles always led to a loss of controllability over longer time periods, consistent with the fixed-phase feedback results. The Fig. 10e vorticity is very similar to the fixed-phase feedback vorticity distribution shown in Fig. 6c. The recirculation zone is clearly lengthened in the stabilized flow, which leads to a decrease in the vortex-shedding frequency by 23% (Fig. 10b).

The drag and unsteady lift force reduction manifests itself in a change in the mean flow, as well as the rms distribution. Figure 11 shows a comparison of the unforced mean flow and rms distributions to those encountered in the stabilized feedback-controlled state, between 6 and 8 s, in the feedback-controlled run presented in Fig. 10. The recirculation zone length has almost doubled in length, and the peak in the rms distribution is shifted from $x/D = 2.5$ to $x/D = 5$. Also, it can be seen that the controlled wake up to 3 diameters downstream of the cylinder is entirely steady.

Whereas in the run shown in Fig. 10 the phase advance was a combined result of the dense localized sensor placement and the variable-gain feedback, the same effect can be achieved using a global sensor field as the one shown in Fig. 2 in combination with a suitable, nonlinear variable-phase advance based on the nonfluctuating mode 5 only. This would be an extension to Eq. (5) by adding a nonlinear term to the adjustment of the controller phase shift. We find that a variable-gain strategy that adjusts the feedback gains according to the change in the mean flow achieves better results than a fixed-gain control approach. One would expect that the largely modified feedback-controlled flowfield, where the vortex shedding has shifted significantly downstream, would require a different feedback gain due to the different spatial separation between the location where actuation is applied, fixed at the cylinder, and the location where the flow needs to be controlled by the actuation, the vortex formation location that has shifted in the downstream direction. This consideration may be used to explain the success of the variable-gain strategy because the initial feedback gain and phase, as well as any fixed gains, is optimized for the uncontrolled flowfield and recirculation zone length. Because the vortex formation location has shifted downstream, one would expect that more actuation is needed for the feedback-controlled flow because the actuation input is subject to more viscous damping as it is convected downstream. By the same argument, the phase of the actuation needs to be adjusted such that it compensates for the time delay encountered due to the longer convection from the actuator to the vortex formation location. The variable-gain feedback approach accomplishes both of these objectives, thus maintaining control over the vortex shedding.

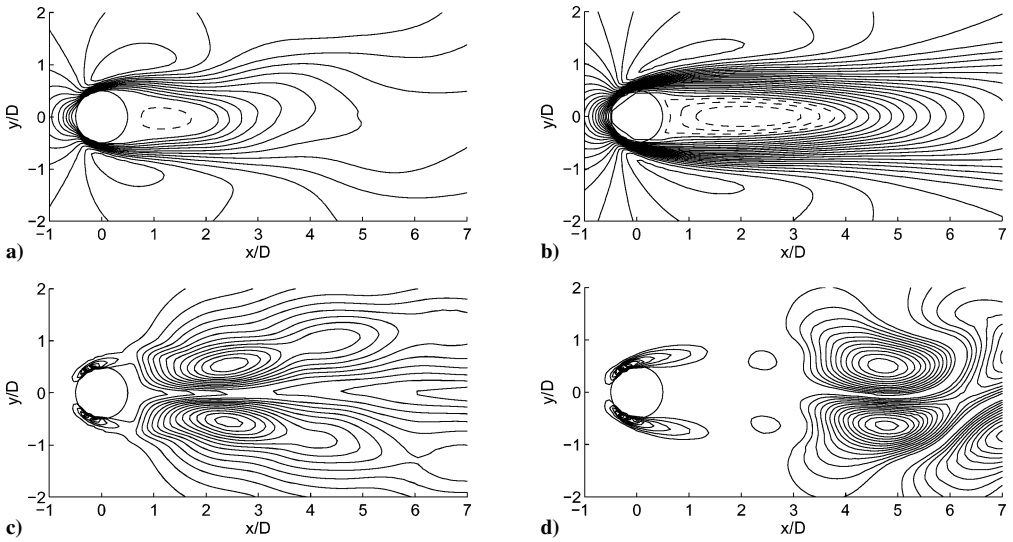

Fig. 11 Cylinder centered at (0, 0) and of diameter 1, flow from left to right: ——, positive isocontours and – – –, negative isocontours: a) and b) mean flow and c) and d) rms velocity distributions; left, uncontrolled and right, controlled case using variable gain of Fig. 10.

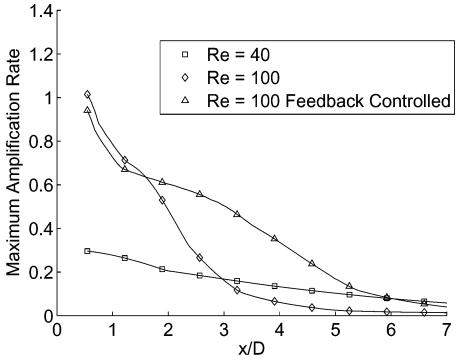

Fig. 12 Linear stability analysis of unforced and feedback-controlled flowfield in Fig. 10.

When feedback control is applied, significant changes in the mean flowfield occur, as shown in the preceding section. Therefore, it is of interest to investigate how the stability characteristics of the mean flow are modified as a result of the mean flow changes. Linear stability analysis based on numerical solution of the Orr–Sommerfeld equations using spectral methods (Trefelthen[33]) was used to analyze these changes. Figure 12 shows a comparison of the maximum growth rate of the unforced flowfield at a Reynolds number of 100 to the steady-state feedback controlled flowfield shown in Fig. 10. Despite the fact that the near-wake fluctuations are suppressed by the feedback, as shown in the preceding section, the flowfield has become more unstable beyond two diameters downstream of the cylinder. Comparing the unforced flow to a stable flow field at a subcritical Reynolds number of 40, one can see that the von Kàrmàn vortex street at $Re = 100$ leads to a more stable flowfield beyond $x/D = 3$.

Discussion

We used POD as a tool to process multiple sensor signals into a global estimate of the flow state. POD allows for stable global wake state estimation, enables multisensor evaluation, and eliminates artifacts of local sensing, that is, sensing at nodes of the vortex street. It also allows for an accurate state estimate when the effect of the controller causes major changes both in the mean flow and the rms amplitudes of the fluctuating velocity components. However, we find it necessary to account for the changes in the mean flow by adding a mean flow mode (mode 5) to the model.

Although we used only mode 1 for closing the feedback loop, all of the higher-order POD modes experienced reductions in mode amplitude, even a larger relative reduction than the von Kàrmàn mode used for feedback. This is quantitatively shown in Table 1.

Table 1 Mode amplitude reductions achieved using variable-gain feedback with parameters in Fig. 10

Mode	Unforced amplitude, m/s	Feedback-controlled amplitude, m/s	Amplitude reduction, %
1	100	50	50
2	90	45	50
3	22	6.75	69
4	21.5	6.5	70

The larger reduction of the higher-order modes suggests a strong coupling between all modes and implies that the existence of the higher-order modes is conditional on the presence of the fundamental modes. This confirms the results of our previous work.[14]

Although feedback control was able to stabilize the near wake of the cylinder, vortex formation still occurred, though farther downstream. Whereas the reasons for this are not entirely clear, we suggest several possible causes. The change in the mean flow caused by the controller lengthens the recirculation zone. This moves the vortex formation location farther downstream and causes a reduction in both drag and rms lift force. Whereas both of these effects are desired, the downstream shift in vortex formation location causes a larger spatial separation between the actuation, which remains at the cylinder, and the oscillations the actuator attempts to cancel. This requires both more actuation input and also an adjustment in the actuation phase to account for the time a given disturbance takes to travel from the actuator to the vortex formation location. At the same time, the disturbances caused by the actuator need to travel through a region of the flow that, while stabilized, is only stabilized within a narrow range of phase angles. If the far wake requires a phase angle for stabilization that at the same time destabilizes the near wake, a physical limit has been reached in terms of what can be achieved given the actuator location. This effect may limit the spatial range for which stabilization can be achieved with the current actuator setup. This is particularly true because the vortex suppression achieved in this investigation decreases the stability of the feedback-controlled flowfield and extends the unstable region of the flow farther downstream of the cylinder, as was demonstrated by the linear stability investigations shown in the preceding section.

Despite all of these problems, we were able to suppress the oscillations in the near wake without directly modifying the mean flow or changing the separation point using, for example, momentum injection. Thus, this effort shows that the cylinder wake flow can be improved in terms of drag and unsteady lift by feedback control. For this reason, one would expect the current control approach to be applicable to wake flows with fixed separation points, such as the flow around a D-shaped cylinder. The same cannot be said for

approaches that aim at moving the separation point aft, for example, by tripping the boundary layer or using blowing and suction upstream of the separation point to delay separation.

In parallel with this paper, Gerhard et al.[34] also employ a low-order model based approach to control the circular cylinder wake. Whereas details of the low-order model, estimation technique, and control algorithm employed are different from our approach, the qualitative effects of the control on the flowfield appear to be very similar. This indicates that the limitations encountered in both of our control approaches may be inherent to actuation authority and inherent to the physics of the flowfield itself. (Note that both approaches use a localized actuation in a small portion of the flowfield.)

Overall, we were able to reduce the effect of vortex shedding on both the unsteady lift and the vortex-induced portion of the pressure drag by about an order of magnitude.

Recommendations

Although this investigation demonstrates the potential that feedback flow control offers in terms of reducing unsteady lift and drag of a bluff body at low Reynolds numbers, it is unclear what the results of applying the control approaches employed in this research at higher Reynolds numbers will be. Unforced CFD simulations at a Reynolds number of 160 show that the vortex-induced drag portion of the overall drag increases from 16% at $Re = 100$ to more than 30% at $Re = 160$. This indicates that the same control approach at higher Reynolds numbers may yield larger decreases in drag. However, this must be investigated in detail in future research. Additionally, we still have to close the feedback loop experimentally. This will be the ultimate test for the applicability of the simulation results.

Summary

The wake of a circular cylinder at $Re = 100$ was feedback controlled in a two-dimensional CFD simulation using a low-dimensional-model-based state estimation of the near wake. Using a variable gain linear feedback of the first von Kármán mode, we were able to reduce the unsteady lift fluctuations as well as the vortex-induced portion of the lift by about one order of magnitude. As a result of the feedback, the length of the time-averaged recirculation zone doubled. Whereas the feedback-controlled near wake was entirely steady, the flow beyond $x/D = 3$ still exhibited some slight unsteadiness.

Acknowledgments

The authors acknowledge funding for this research from the Air Force Office of Scientific Research, Program Monitor Belinda B. King. We also acknowledge the fruitful discussions and information exchange with Gilead Tadmor and Bernd R. Noack. We thank Bill Strang and Jim Forsythe from Cobalt, LLC, for their support in providing the computational fluid dynamics tools.

References

[1]Williamson, C. H. K., "Vortex Dynamics in the Cylinder Wake," *Annual Review of Fluid Mechanics*, Vol. 28, 1996, pp. 477–539.

[2]Karniadakis, G., and Triantafyllou, G. S., "Three-Dimensional Dynamics and Transition to Turbulence in the Wake of Bluff Bodies," *Journal of Fluid Mechanics*, Vol. 238, 1992, pp. 1–30.

[3]Roussopoulos, K., "Feedback Control of Vortex Shedding at Low Reynolds Numbers," *Journal of Fluid Mechanics*, Vol. 248, 1993, pp. 267–296.

[4]Park, D. S., Ladd, D. M., and Hendricks, E. W., "Feedback Control of von Kármán Vortex Shedding Behind a Cylinder at Low Reynolds Numbers," *Physics of Fluids*, Vol. 6, No. 7, 1994, pp. 2390–2405.

[5]Monkewitz, P. A., "Modeling of Self-Excited Wake Oscillations by Amplitude Equations," *Experimental Thermal and Fluid Science*, Vol. 12, No. 2, 1996, pp. 175–183.

[6]Blevins, R., *Flow Induced Vibration*, 2nd ed., Van Nostrand Reinhold, New York, 1990, pp. 54–58.

[7]Koopmann, G., "The Vortex Wakes of Vibrating Cylinders at Low Reynolds Numbers," *Journal of Fluid Mechanics*, Vol. 28, Pt. 3, 1967, pp. 501–512.

[8]Min, C., and Choi, H., "Suboptimal Feedback Control of Vortex Shedding at Low Reynolds Numbers," *Journal of Fluid Mechanics*, Vol. 401, 1999, pp. 123–156.

[9]Gillies, E. A., "Low-Dimensional Characterization and Control of Non-Linear Wake Flows," Ph.D. Dissertation, Faculty of Engineering, Univ. of Glasgow, Glasgow, Scotland, U.K., June 1995.

[10]Li, F., and Aubry, N., "Reactive Flow Control for a Wake Flow Based on a Reduced Model," AIAA Paper 2000-2531, June 2000.

[11]Bewley, T., and Trenchea, C., "Noncooperative Optimization of Controls for Time-Periodic Navier–Stokes Systems (Invited)," AIAA Paper 2002-2754, June 2002.

[12]Deane, A. E., Kevrekidis, I. G., Karniadakis, G. E., and Orszag, S. A., "Low-Dimensional Models for Complex Geometry Flows: Application to Grooved Channels and Circular Cylinders," *Physics of Fluids*, Vol. 3, No. 10, 1991, pp. 2337–2368.

[13]Gillies, E. A., "Low-Dimensional Control of the Cylinder Wake," *Journal of Fluid Mechanics*, Vol. 371, 1998, pp. 157–178.

[14]Cohen, K., Siegel, S., McLaughlin, T., and Gillies, E., "Feedback Control of a Cylinder Wake Low Dimensional Model," *AIAA Journal*, Vol. 41, No. 7, 2003, pp. 1389–1391.

[15]Ma, X., and Karniadakis, G., "A Low-Dimensional Model for Simulating Three-Dimensional Cylinder Flow," *Journal of Fluid Mechanics*, Vol. 458, 2002, pp. 181–190.

[16]Newman, D. J., and Karniadakis, G. E., "Simulations of Flow over a Flexible Cable: A Comparison of Forced and Flow-Induced Vibrations," *Journal of Fluids and Structures*, Vol. 10, No. 5, 1996, pp. 439–453.

[17]Strang, W. Z., Tomaro, R. F., and Grismer, M. J., "The Defining Methods of Cobalt60: A Parallel, Implicit, Unstructured Euler/Navier–Stokes Flow Solver," AIAA Paper 99-0786, Jan. 1999.

[18]Gottlieb, J. J., and Groth, C. P. T., "Assessment of Riemann Solvers for Unsteady One-Dimensional Inviscid Flows of Perfect Gases," *Journal of Computational Physics*, Vol. 78, No. 2, 1988.

[19]Karypis, G., Schloegel, K., and Kumar, V., "ParMETIS: Parallel Graph Partitioning and Sparse Matrix Ordering Library Version 1.0," Dept. of Computer Science, Univ. of Minnesota, Minneapolis, MN, July 1997.

[20]Grismer, M. J., Strang, W. Z., Tomaro, R. F., and Witzemman, F. C., "Cobalt: A Parallel, Implicit, Unstructured Euler/Navier–Stokes Solver," *Advances in Engineering Software*, Vol. 29, No. 3–6, 1998, pp. 365–373.

[21]Kotapati-Apparao, R., Forsythe, J., and Squires, K., "Computation of the Flow Over a Maneuvering Spheroid," AIAA Paper 2003-0269, Jan. 2003.

[22]Viswanathan, A., Klismith, K., Forsythe, J., and Squires, K., "Detached-Eddy Simulation Around a Rotating Forebody," AIAA Paper 2003-0263, Jan. 2003.

[23]Oertel, H., Jr., "Wakes Behind Blunt Bodies," *Annual Review of Fluid Mechanics*, Vol. 22, 1990, pp. 539–564.

[24]Panton, R. L., *Incompressible Flow*, 2nd ed., Wiley, New York, 1996, pp. 384–400.

[25]Holmes, P., Lumley, J. L., and Berkooz, G., *Turbulence, Coherent Structures, Dynamical Systems and Symmetry*, Cambridge Univ. Press, Cambridge, England, U.K., 1996, pp. 86–127.

[26]Sirovich, L., "Turbulence and the Dynamics of Coherent Structures Part I: Coherent Structures," *Quarterly of Applied Mathematics*, Vol. 45, No. 3, 1987, pp. 561–571.

[27]Smith, D. R., Siegel, S., and McLaughlin, T., "Modeling of the Wake Behind a Circular Cylinder Undergoing Rotational Oscillation," AIAA Paper 2002-3066, June 2002.

[28]Noack, B. R., Afanasiev, K., Morzynski, M., and Thiele, F., "A Hierarchy of Low-Dimensional Models for the Transient and Post-Transient Cylinder Wake," *Journal of Fluid Mechanics*, Vol. 497, 2003, pp. 335–363.

[29]Adrian, R. J., "On the Role of Conditional Averages in Turbulence Theory," *Proceedings of the Fourth Biennial Symposium on Turbulence in Liquids*, edited by J. Zakin and G. Patterson, Science Press, Princeton, NJ, 1977, pp. 323–332.

[30]Bonnet, J. P., Cole, D. R., Delville, J., Glauser, M. N., and Ukeiley, L. S., "Stochastic Estimation and Proper Orthogonal Decomposition: Complementary Techniques for Identifying Structure," *Experiments in Fluids*, Vol. 17, No. 5, 1994, pp. 307–314.

[31]Williamson, C. H. K., and Roshko, A., "Vortex Formation in the Wake of an Oscillating Cylinder," *Journal of Fluids and Structures*, Vol. 2, July 1988, pp. 355–381.

[32]Ahlborn, B., Seto, M., and Noack, B., "On Drag, Strouhal Number and Vortex Street Structure," *Fluid Dynamics Research*, Vol. 30, 2002, pp. 379–399.

[33]Trefelthen, L. N., *Spectral Methods in MATLAB*, Society for Industrial and Applied Mathematics, Philadelphia, 2000, pp. 145–152.

[34]Gerhard, J., Pastoor, M., King, R., Noack, B., Dillman, A., Morzynski, M., and Tadmor, G., "Model-Based Control of Vortex Shedding Using Low-Dimensional Galerkin Models," AIAA Paper 2003-4262, June 2003.

K. Ghia
Associate Editor